

A STUDY OF THE PHENOMENON BUE CREATION IN TROCHOIDAL MILLING

NAVARIT WINNUWAT¹, APIWAT MUTTAMARA¹, JIRAWAN KLOYPAYAN¹

¹Faculty of Engineering, Thammasat School of Engineering (TSE), Thammasat University, Pathumthani 12120, Thailand

DOI: 10.17973/MMSJ.2023_06_2022161

navarit.winn@dome.tu.ac.th

Aluminum alloy 6061-T6 is a commonly used material in various industries, including automotive parts manufacturing. However, its machining process can be challenging due to the occurrence of built-up edge (BUE) at the cutting edges. To address this issue, this research employed trochoidal milling to machine aluminum alloy 6061-T6 specimens, utilizing a small step over and a suitable depth of cut. The engagement of the tool during the machining process generates fluctuating forces, which consequently leads to fluctuations in temperature. This phenomenon is not only observed in trochoidal milling but also in conventional machining methods. The results indicate that the calculated maximum temperature (350°C) is lower than the aluminum's melting point (652°C). Moreover, the experimental results show minimal BUE formation on the cutting edge and an improved milling process.

KEYWORDS

Trochoidal milling, Cutting force and Build up edge (BUE)

1 INTRODUCTION

Aluminum processing has become increasingly prevalent in the industry due to its durability and lightweight nature. Some of the typical properties of aluminum include a density of only 2.7g/cm³, an elongation of 5%, a melting point of 652°C, a vaporization temperature of 1800°C, and a specific heat of 25. Its crystal structure is Face-Centered Cubic (FCC), making it ductile even at low temperatures, which increases its strength without compromising its quality. Aluminum is an excellent electrical conductor, with a conductivity of approximately 62% that of copper, but weighing less than a third of it. This makes it an economical material compared to other metals such as steel (7.83g/cm³), copper (8.93g/cm³), or brass (8.53g/cm³). Its non-sparking and non-magnetic characteristics make it essential for products used in highly flammable or explosive environments. Aluminum is also an excellent heat conductor, making it important for heat exchange applications, whether for heating or cooling. It is commonly used in the food, chemical, petroleum, aircraft, and automotive industries. The aluminum alloy 6061-T6 used in this study has specific properties and chemical composition as shown in Tab. 1, Tab. 2. Additionally, aluminum alloy 6061-T6 exhibits excellent corrosion resistance and possesses the ability to dissipate heat quickly in normal and high-temperature environments. Furthermore, it has high hardness and is widely used in the production of mechanical parts and various molds. There are two primary methods for milling processes: orthogonal milling and oblique milling. The cutting principle refers to a method in which the chip is formed along the shear plane during the cutting process. Trochoidal milling is a type of oblique milling that involves removing small steps with

a deep cut. The cutting force and temperature are lower in trochoidal milling compared to conventional methods, even at the same axial depth of cut. As a result, BUE formation is a common problem encountered during the milling of aluminum alloy 6061-T6. [Hasan et al 2008] reported that the formation of built-up edge (BUE) and build-up layer (BUL) had a positive effect on cutting forces and surface roughness, particularly at lower cutting speeds. [Bhowmick et al 2010] noted that the utilization of minimum quantity lubrication (MQL) can prevent the adherence of tools and the formation of built-up edge (BUE), thereby extending tool life and reducing force and torque compared to dry conditions. [Fang et al 2010] reported that the initiation region of built-up edge (BUE), where BUE begins to form and the magnitude of vibration changes significantly, varies with cutting speed. [Atlati et al 2015] observed that an increase in the local friction coefficient resulted in a significant rise in the plastic strain at the secondary shear zone, leading to the generation of a volumetric heat source. This, in turn, caused an increase in the cutting temperature and subsequently facilitated the adhesion of the work material on the rake face. Consequently, the formation of built-up edge (BUE) occurred. [A. Agic et al 2016] reported that the increase in the rate of tangential cutting force may be attributed to the sudden growth of the chip load area during nose corner engagement. [U.A.A. et al 2017] reported that the presence of cutting fluid in the cutting zone can decrease the formation of built-up edge (BUE). The primary objective of this research was to investigate the heat generated during trochoidal milling of aluminum alloy 6061-T6. The cutting force and cutting temperature are correlated because as the cutting edge penetrates the workpiece, heat is generated, causing an increase in the cutting edge temperature. The study aimed to analyze this correlation and identify the factors that affect the formation of BUE to improve the milling process's tool life. This relationship between cutting force and cutting temperature is described by the Johnson and Cook constitutive model, where the stress σ varies with time t . By using this model, it is possible to establish the relationship between cutting force and cutting temperature. This relationship is important in understanding the behavior of the machining process and can provide insights into the mechanism of material removal during cutting. Therefore, this research aims to analyze the various factors that affect the formation of the built-up edge, with a focus on achieving a long lifespan for the cutting tool.

Hardness (Rockwell Scale B)	Young's Modulus (GPa)	Yield Strength (MPa)
60	69	275
Tensile Strength (MPa)	Thermal Expansion Coefficient ($\mu\text{m}/\text{m}^{\circ}\text{C}$)	Thermal Conductivity (W/mK)
310	23.6	167

Table 1. Aluminum alloy 6061-T6 properties

Si (wt.%)	Fe (wt.%)	Cu (wt.%)	Mn (wt.%)	Mg (wt.%)	Zn (wt.%)
0.340	0.509	0.151	0.701	1.17	0.0044
Cr (wt.%)	S (wt.%)	Ti (wt.%)	Sb (wt.%)	Ni (wt.%)	Al (wt.%)
0.0102	< 0.005	0.0625	< 0.0625	0.00778	98.94

Table 2. Chemical composition of aluminum alloy

2 ANALYSIS OF TROCHOIDAL MILLING

2.1 Nominal instantaneous uncut chip thickness

The analysis of instantaneous uncut chip thickness model of conventional milling can be expressed by Yanjie Yuan 's analysis [Yanjie et al 2018] of the movement of the tool with two cutting

edges in trochoidal milling in Fig. 1. The cutting edge location $(x(k), y(k))$ of trochoidal milling can be calculated by Eq. (1).

$$x(k) = \frac{ft}{60} + R \sin\left(\omega t - \frac{2\pi k}{K}\right) + r_0 \sin(\omega t + \lambda)$$

$$y(k) = R \cos\left(\omega t - \frac{2\pi k}{K}\right) + r_0 \cos(\omega t + \lambda) \quad (1)$$

where k is the tooth number, K is the number of teeth, λ is a phase angle, f is the feed rate (mm/min), ω is the spindle angular velocity (rad/s), t is time (s), and r_0 is the movement of tool in a trochoidal milling process. The nominal uncut chip thickness h_n as shown in Fig. 1 can be calculated as illustrated in Eq. (2).

$$h_n = H - R_m = R + L \sin\left(\omega t_k - \frac{2\pi k}{K} + \alpha_0\right) - \sqrt{R^2 - L^2 \cos^2\left(\omega t_k - \frac{2\pi k}{K} + \alpha_0\right)} \quad (2)$$

where H is the perpendicular distance of the previous line to the next line, t is the time of tool movement, R_m is the distance between the perpendicular of the previous line to the cutting edge position, R is a radius of cutting tool, L is the distance between the center of the tool at the previous position to the next position as illustrated in Eq. (3), ω is angular velocity, t_k is the time that the cutting edge moves while cutting workpiece, k is the tooth number, K is the number of teeth, α_0 is the angle between the two tool center points at the previous position (x_{k-m}, y_{k-m}) and the next position (x_k, y_k) corresponding to time as illustrated in Eq. (4).

$$L = \sqrt{(x_k - x_{k-m})^2 + (y_k - y_{k-m})^2} \quad (3)$$

$$\alpha_0 = \arctan\left(\frac{y_k - y_{k-m}}{x_k - x_{k-m}}\right) \quad (4)$$

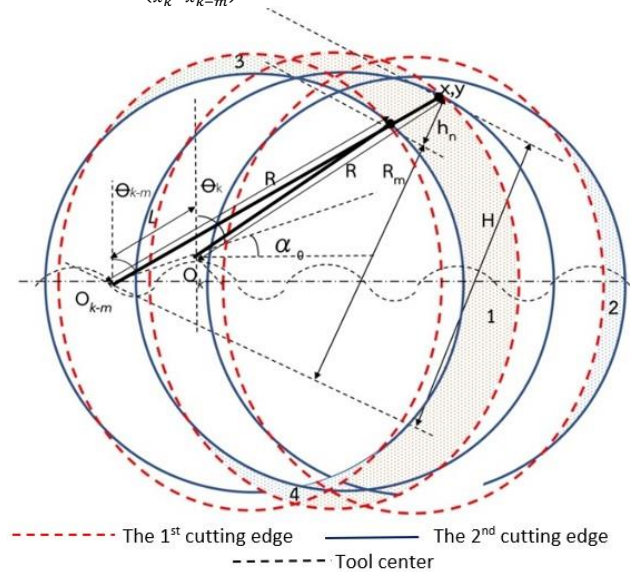


Figure 1. Nominal instantaneous uncut chip thickness calculation geometry

2.2 Cutting force in trochoidal milling

Cutting force is composed of tangential (dF_t), radial (dF_r) and axial (dF_a) forces can be modeled as illustrated in Eq. (5).

$$\begin{aligned} dF_t(t) &= [K_{tc}h_n(\theta) + K_{te}]dz \\ dF_r(t) &= [K_{rc}h_n(\theta) + K_{re}]dz \\ dF_a(t) &= [K_{ac}h_n(\theta) + K_{ae}]dz \end{aligned} \quad (5)$$

where the cutting angle θ (rad) is defined by Eq. (6).

$$\theta = \arccos\left(\frac{R-h_n}{R}\right) \quad (6)$$

and K_{tc} , K_{rc} , K_{ac} are the cutting force coefficients in the tangential, radial and axial direction, respectively. K_{te} , K_{re} and K_{ae} are the corresponding edge force coefficients [Yanjie et al 2018] and dF_x , dF_y and dF_z can be modeled as shown in Eq. (7).

$$dF_x(t) = \{-[K_{tc}h_n(\theta) + K_{te}] \cos \theta - [K_{rc}h_n(\theta) + K_{re}] \sin(\theta)\}dz$$

$$dF_y(t) = \{[K_{tc}h_n(\theta) + K_{te}] \sin \theta - [K_{rc}h_n(\theta) + K_{re}] \cos \theta\}dz$$

$$dF_z(t) = [K_{ac}h_n(\theta) + K_{ae}]dz \quad (7)$$

The cutting force in X, Y and Z axis can be calculated as illustrated in Eq. (8). Then, the resultant force (F) is calculated as illustrated in Eq. (9).

$$F_x(t) = \frac{R}{\tan \beta} \sum_{i=1}^i \int_{\theta_b}^{\theta_t} \{-[K_{tc}h_n(\theta) + K_{te}] \cos \theta - [K_{rc}h_n(\theta) + K_{re}] \sin \theta\}d\theta$$

$$F_y(t) = \frac{R}{\tan \beta} \sum_{i=1}^i \int_{\theta_b}^{\theta_t} \{[K_{tc}h_n(\theta) + K_{te}] \sin \theta - [K_{rc}h_n(\theta) + K_{re}] \cos \theta\}d\theta$$

$$F_z(t) = \frac{R}{\tan \beta} \sum_{i=1}^i \int_{\theta_b}^{\theta_t} [K_{ac}h_n(\theta) + K_{ae}]d\theta \quad (8)$$

$$F = \sqrt{F_x^2 + F_y^2 + F_z^2} \quad (9)$$

2.3 Cutting temperature

The cutting temperature (T) of aluminum alloy 6061-T6 can be calculated by the Johnson and Cook constitutive model in Eq. (10). Cutting temperature can be calculated as shown in Eq. (11). A , B and C are material model constants for aluminum alloy 6061-T6 as shown in Tab. 3 [Daoud et al 2015]. They obtained from cylinder impact test in Al 60061-T6. The test data are primarily obtained from torsion test over a wide range of strain rates (quasi-static to about $400s^{-1}$) and dynamic Hopkinson bar tensile tests over a range of temperatures. Static tensile data are also used. The five material constants are A , B , C , n and m . A is the yield stress, B and n represent the effects of strain hardening, C is strain rate constraint, m is thermal softening data obtained from Hopkinson bar test.

$$\sigma = (A + B(\epsilon)^n) \left(1 + C \ln \frac{\dot{\epsilon}}{\dot{\epsilon}_0}\right) \left(1 - \left(\frac{T - T_{room}}{T_{melt} - T_{room}}\right)^m\right) \quad (10)$$

$$T = \left[T_{melt} - T_{room}\right] \left(m \sqrt{1 - \frac{\sigma}{(A+B(\epsilon)^n)(1+C \ln \frac{\dot{\epsilon}}{\dot{\epsilon}_0})}}\right) + T_{room} \quad (11)$$

A (MPa)	B (MPa)	C (MPa)	n	m	Plastic Strain (ϵ)
250	79	0.0249	0.499	1.499	0.86
Plastic Strain Rate ($\dot{\epsilon}$)			Reference Plastic Strain Rate ($\dot{\epsilon}_0$)		
597.2			1		
Material Melting Temperature (T_{melt}) ($^{\circ}C$)			Room Temperature (T_{room}) ($^{\circ}C$)		
652			30		

Table 3. Constants of aluminum alloy 6061-T6

The shear stress, S_s can be obtained from the tensile stress, σ as illustrated in Eq. (12).

$$S_s = \frac{\sigma}{\sqrt{3}} \quad (12)$$

where S_s is shear stress and σ is tensile stress by using the von Mises criterion and the Johnson-Cook material model as shown in Eq. (10).

3 EXPERIMENTAL PROCEDURES

In this experiment, we utilized a CNC vertical machining center, specifically the Eumach Model LMC 1020. The workpieces utilized were made of aluminum alloy 6061-T6, with dimensions of 40 x 40 x 150mm, as depicted in Fig. 2. The workpieces were precisely positioned and machined using a cobalt high-speed cutting tool. An uncoated cutting tool (Nachi Model 2SE LIST 6230 10X25X75X10 SA17 HSS-Co) with two fluted cutting edges was used, with a diameter of 10mm, length of 75mm, and cutting

length of 25mm is illustrated in Fig. 3. Fig. 4 displays a cutting segment of cutting tool, while Fig. 5 displays the geometry of cutting tool. Fig. 6 depicts the direction of each cutting force exerted on the cutting edge during the process of cutting the workpiece. Cutting force was measured using a dynamometer (Kistler 9272), as illustrated in Fig. 7. A 150mm long workpiece after being cut is depicted in Fig. 8. Cutting parameters used in the milling process are listed in Tab. 4.

Cutting Length (mm)	Spindle Speed (rev/min)	Feed rate (mm/min)
150	1900	450
The movement of tool in a trochoidal milling (r_o) (mm)		Depth of cut (a_p) (mm)
0.8		5
2.4		10

Table 4. Cutting parameters

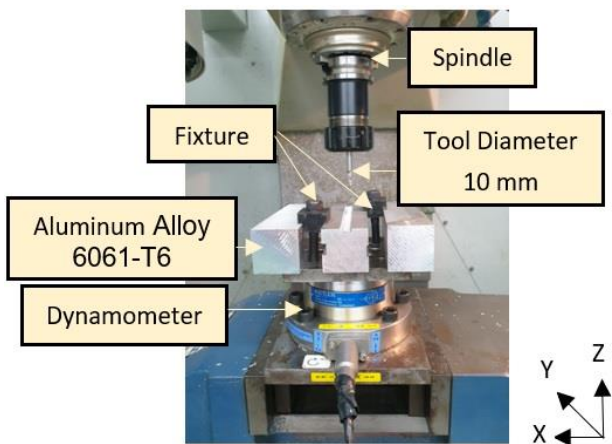


Figure 2. Spindle with cutting tool, workpieces and dynamometer

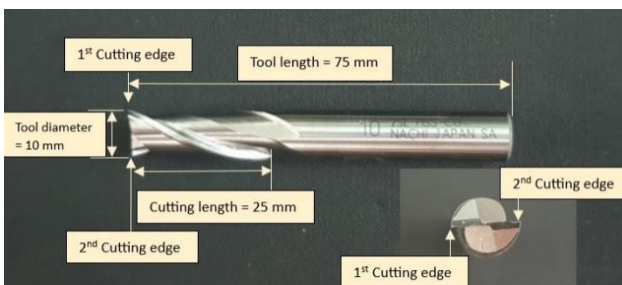


Figure 3. Geometry of cutting tool

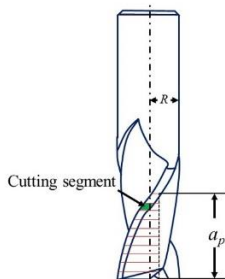


Figure 4. Cutting segment of cutting tool

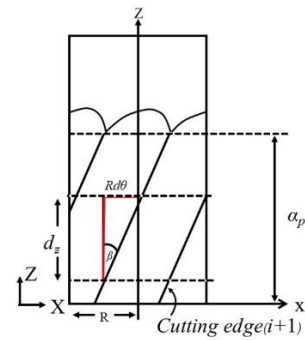


Figure 5. Geometry of cutting tool

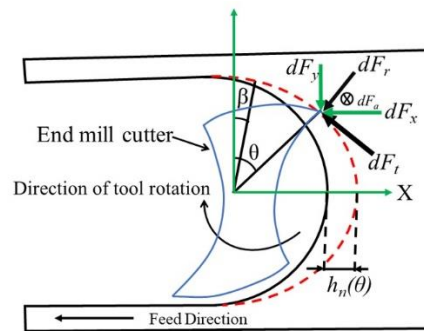


Figure 6. Schematic diagram of cutting tool process

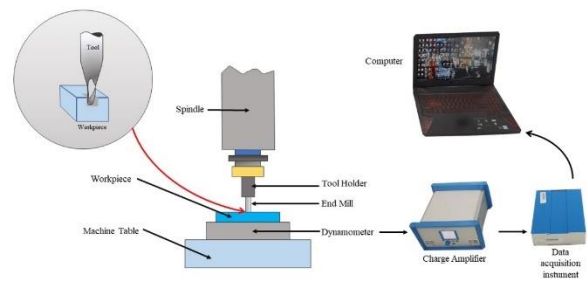


Figure 7. Schematic diagram of experimental set up

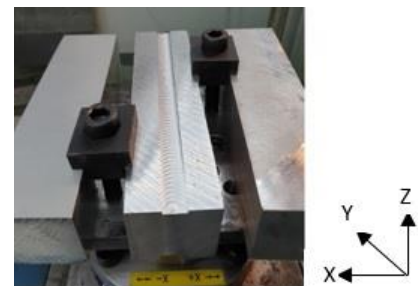


Figure 8. Workpiece after being cut

4 EXPERIMENTAL RESULTS

Fig. 9 and 12 illustrate a comparison between the cutting forces calculated using Matlab R2022b and the experimentally measured cutting forces using the Kistler 9272 dynamometer. The results demonstrate a close similarity between the calculated and measured cutting forces. Meanwhile, Fig. 10 and 13 depict the uncut chip thickness, which varies based on the engagement of the cutting edges as shown in Fig. 1. Additionally, Fig. 11 and 14 demonstrate the trochoidal trajectory of cutting tool. The analysis indicates that the simulation and experimental results exhibit a similar trend in the cutting forces.

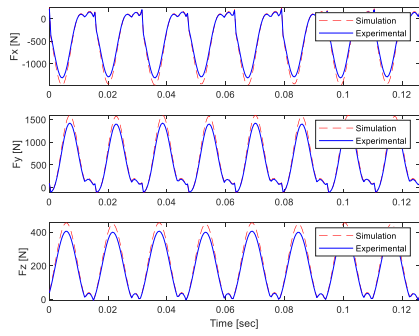


Figure 9. Cutting force in x, y and z axis ($r_o = 0.8\text{mm}$, $a_p = 5\text{mm}$)

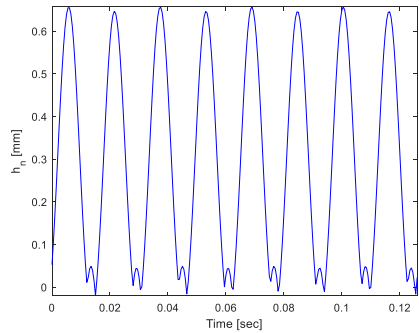


Figure 10. Nominal uncut chip thickness ($r_o = 0.8\text{mm}$, $a_p = 5\text{mm}$)

The cutting force fluctuates depending on the position of the cutting edge during engagement with the workpiece. The comparison between Fig. 9 and Fig. 12, it was observed that the cutting force exerted in Fig. 12 is greater than that in Fig. 9 across all axes. This difference in cutting force can be attributed to the higher values of r_o and a_p depicted in Fig. 12.

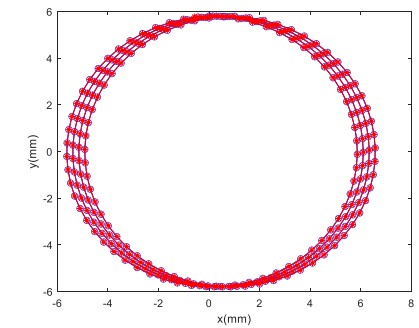


Figure 11. Trajectory of cutting tool ($r_o = 0.8\text{mm}$, $a_p = 5\text{mm}$)

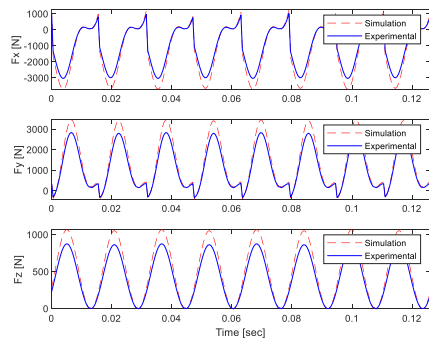


Figure 12. Cutting force in x, y and z axis ($r_o = 2.4\text{mm}$, $a_p = 10\text{mm}$)

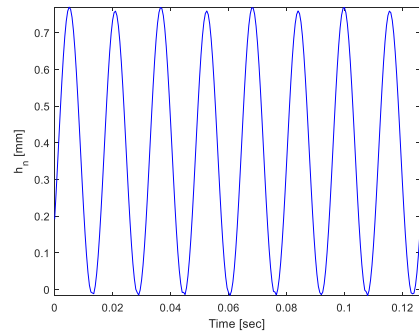


Figure 13. Nominal uncut chip thickness ($r_o = 2.4\text{mm}$, $a_p = 10\text{mm}$)

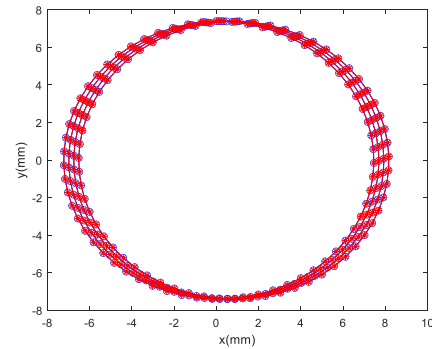


Figure 14. Trajectory of cutting tool ($r_o = 2.4\text{mm}$, $a_p = 10\text{mm}$)

The star line in Fig. 16 and Fig. 17 represents the assumed temperature measurement on the surface of the tool outside the cutting zone using a thermal scanning camera, as illustrated in Fig. 15. Measurements utilizing a thermal scanning camera involve capturing images of the cutting edge of the cutter during the cutting process. The heat generated as a result of this cutting action is then measured as a temperature on the surface of the cutting area outside of the cutting tool. To capture these temperature readings, a thermal scanning camera is positioned and held steady while the cutting is in progress. The brand and model of the thermal scanning camera used in the experiment is as follows: FLIR T420 320 x 240 Pixel Resolution, MSX-enabled, <0.5deg C, 25deg x 19deg field of view infrared camera. The thermal scanning camera should be positioned at a distance of approximately 500mm from both the workpiece and the cutting tool during the cutting process, in order to accurately measure and monitor the temperature. In order to perform a calibration test, it is necessary to deploy targets with known temperatures. Two of the most commonly used reference points are melting ice and boiling water. Ensuring that these reference points reflect their known temperatures as accurately as possible is crucial for achieving precise infrared camera heat signatures. To assess the specifications of a thermal scanning camera, a reading within the range of +/-2°C is considered acceptable for both boiling water (98°C - 102°C or 208.4°F - 215.6°F) and melting ice. This level of accuracy is deemed acceptable based on the camera's technical specifications. Trochoidal milling is a machining process that is designed to achieve smaller undeformed chip thickness, thereby reducing cutting forces. During the cutting process, the cutting edge moves forward, cutting the workpiece. The maximum temperature was equal to 350°C which is lower than the melting temperature of aluminum (652°C). The star line shows the temperature of the workpiece measured by the thermal scanning camera, while cutting. The results show that the actual temperatures are lower than the simulation because the measured temperature was not measured at the actual cutting edge, but measured on the surface of the tool outside the cutting zone. The discrepancy between measured and simulated temperatures will be

influenced by the variation in temperature data. The measured temperature gradually increased at the beginning of the milling process, then became constant at the maximum temperature of 150°C because of the accumulation of cutting heat generated. The temperature from the cutting heat generate was also much lower than the melting point of the aluminum alloy 6061-T6.



Figure 15. Temperature measurement on the surface of the tool outside the cutting zone using a thermal scanning camera

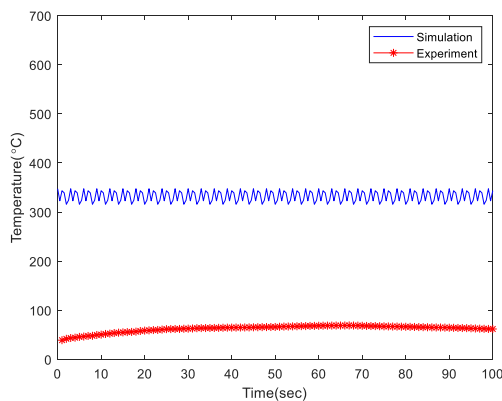


Figure 16. Comparison of temperature between trochoidal cutting by simulation and experiment ($r_o = 0.8\text{mm}$, $a_p = 5\text{mm}$)

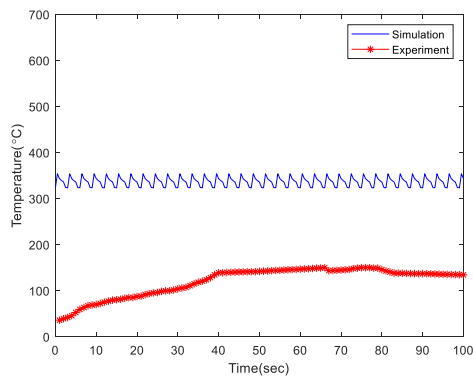


Figure 17. Comparison of temperature between trochoidal cutting by simulation and experiment ($r_o = 2.4\text{mm}$, $a_p = 10\text{mm}$)

In Fig. 18, a build-up edge (BUE) formation can be observed on the cutting tool's edge while using ($r_o = 0.8\text{mm}$, $a_p = 5\text{mm}$), viewed under 200X magnification. The BUE formation was observed to occur in a small region. Similarly, Fig. 19 also depicts a BUE formation in a small area while using ($r_o = 2.4\text{mm}$, $a_p = 10\text{mm}$), as viewed under 200X magnification. Due to the increased workpiece engagement, the BUE formation in Fig. 19 is more extensive than in Fig.18, resulting in more BUE formation at the cutting edge. Although Fig. 19 depicts a cutting edge with BUE formation, it can still be utilized for continued cutting of workpieces. Trochoidal milling is a viable method for milling aluminum with deep cuts without causing damage to the cutting tool.

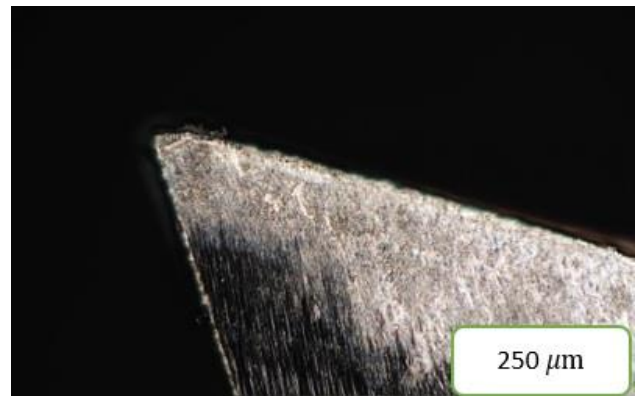


Figure 18. Build up edge on tool edge ($r_o = 0.8\text{mm}$, $a_p = 5\text{mm}$)

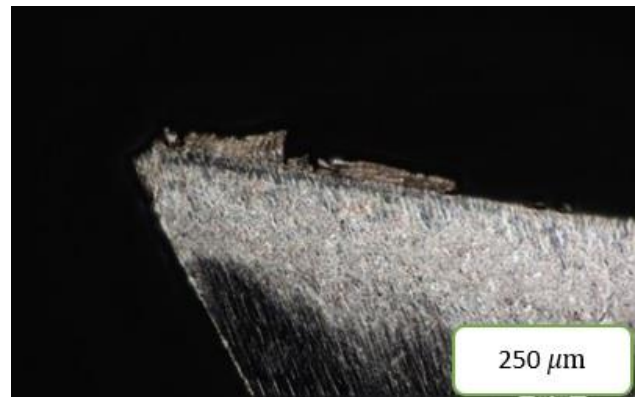


Figure 19. Build up edge on tool edge ($r_o = 2.4\text{mm}$, $a_p = 10\text{mm}$)

5 CONCLUSIONS

This research used trochoidal milling to cut aluminum alloy 6061-T6 specimens. The trochoidal milling engaged a small area of the workpiece with a deep cut, which caused fluctuating force. The maximum forces generated the maximum heat at the cutting edge at much lower temperature than the melting temperature of aluminum. The maximum calculated temperature at the cutting edge would 350°C. It has been demonstrated that under specific conditions, BUE can also be created in trochoidal milling. Therefore, careful adjustment of the process and cutting conditions is crucial. This study not only applies to aluminum alloy 6061-T6, but the findings can also be modified and utilized for cutting other materials. The results of this research on trochoidal milling are anticipated to offer valuable insights and serve as a beneficial reference for upcoming cutting applications.

ACKNOWLEDGMENTS

The authors would like to express their gratitude to the Faculty of Engineering at Thammasat School of Engineering (TSE) for providing a graduate scholarship and supporting this research. Additionally, special thanks are extended to Ms. Veeratchaya Lhemtraai and Mr. Chaovalit Maneekuljitprasas for their valuable contributions to this research project.

REFERENCES

- [Hasan et al 2008] Hasan Gokkaya, Ahmet Taskesen. The effects of cutting speed and feed rate on BUE-BUL formation, cutting forces and surface roughness when machining Aa6351(T6) alloy. Journal of Mechanical Engineering, 2008, Vol.54, No.7-8, pp 521-530.
- [Bhowmick et al 2010] Bhowmick S, Lukitsch MK and Alpas AT. Dry and minimum quantity lubrication drilling of cast

magnesium alloy (AM60). *Int J Mach Tools Manuf*, 2010, Vol.50, pp 444-57.

- [Fang et al 2010] Fang N, Srinivasa Pai P and Mosquea S. The effect of build-up edge on the cutting vibration in machining 2024-T351 aluminum alloy. *Int J Adv Manuf Technol*, 2010, Vol.49, pp 63-71.
- [Atlati et al 2015] S.Atlati, B. Haddag, M. Nouari and A. Moufki. Effect of the local friction and contact nature on the Build-Up Edge formation process in machining ductile metals. *Tribology International*, 2015, Vol.90, pp 217-227.
- [Daoud et al 2015] Daoud M, Jomaa W, Chatelain JF, et al. A machining based methodology to identify material constitutive law for finite element simulation. *Int J Adv Manuf Tech*, 2015, Vol.77, pp 2019-2033.
- [A.Agic et al 2016] A. Agic, O. Gutnichenko, M. Eynian and J-E Stahl. Influence of cutting edge geometry on force build-up process in intermittent turning. *Procedia CIRP*, 2016, Vol.46, pp 364-367.
- [U.A.A. et al 2017] U.A.A. Azlan, M. Hadzley, N. Fauzi Tamin, F.M. Noor, A.A. Azhar, M. Rahimi Yusoff and N.Z. Noriman. Observation of build-up edge formation on a carbide cutting tool with machining aluminum alloy under dry and wet conditions. *EDP Sciences MATEC web of conferences*, 2017, Vol.97, pp 1076.
- [Yanjie et al 2018] Yanjie Yuan, Xiubing Jing, Kornel F. Ehmann, Jian Cao and Huaizhong Li. Modeling of cutting forces in micro end-milling. *J Manuf Processes*, 2018, Vol.31, pp 844-858.

CONTACTS:

Navarit Winnuwat

Apiwat Muttamara/Assoc.Prof. Dr.

Jirawan Kloypayan/Asst.Prof. Dr.

Faculty of Engineering, Thammasat School of Engineering (TSE),
Thammasat University, Thailand

99 Moo 18, Phaholyothin Road, Khlongnueng, Khlongluang,
Pathumthani 12120, Thailand

Telephone: +6 2-564-3001-9

e-mail: naarit.winn@dome.tu.ac.th

mapiwat@engr.tu.ac.th

kjirawan@engr.tu.ac.th